Title

Templating Bicarbonate in the Second Coordination Sphere Enhances Electrochemical CO2 Reduction Catalyzed by Iron Porphyrins

Journal

Journal of the American Chemical Society, 144(26)

ISSN

0002-7863

Authors

Derrick, Jeffrey S
Loipersberger, Matthias
Nistanaki, Sepand K
et al.

Publication Date

2022-07-06

DOI

10.1021/jacs.2c02972

Templating Bicarbonate in the Second Coordination Sphere Enhances Electrochemical CO_2 Reduction Catalyzed by Iron Porphyrins

Jeffrey S. Derrick,[1,2] Matthias Loipersberger,[1] Sepand K. Nistanaki,[1] Martin Head-Gordon,[1,2] Eva M. Nichols,[4]* Christopher J. Chang[1,2,3]*

[1]Department of Chemistry, University of California, Berkeley, CA, 94720, USA

[2]Chemical Sciences Division, Lawrence Berkeley National Laboratory, Berkeley, CA, 94720, USA

[3] Department of Molecular and Cell Biology, University of California, Berkeley, CA, 94720, USA

[4] Department of Chemistry, The University of British Columbia, Vancouver, BC, V6T 1Z1, Canada

ABSTRACT: Bicarbonate-based electrolytes are ubiquitous in aqueous electrochemical CO_2 reduction, particularly in heterogenous catalysis, where they demonstrate improved catalytic performance relative to other buffers. In contrast, the presence of bicarbonate in organic electrolytes and its roles in homogenous electrocatalysis remain underexplored. Here, we investigate the influence of bicarbonate on iron porphyrin-catalyzed electrochemical CO_2 reduction. We show that bicarbonate is a viable proton donor in organic electrolyte (pK_a = 20.8 in DMSO) and that urea pendants in the second coordination sphere can be used to template bicarbonate in the vicinity of a molecular iron porphyrin catalyst. The templated binding of bicarbonate decreases its acidity, resulting in a 1500-fold enhancement in catalytic rates relative to unmodified parent iron porphyrin. This work emphasizes the importance of bicarbonate speciation in wet organic electrolytes and establishes second-sphere bicarbonate templating as a design strategy to harness this adventitious acid and enhance CO_2 reduction catalysis.

INTRODUCTION

The capture and conversion of CO_2 as a cheap, abundant C1 building block into value-added chemical products represents a promising solution to global climate challenges.[1–3] The use of electricity to drive the transformation of CO_2 is an attractive strategy[4] but it requires the development of efficient and selective catalysts that facilitate the CO_2 reduction reaction (CO_2RR) over competitive side reactions such as the hydrogen evolution reaction (HER).[5,6] Heterogeneous systems represent some of the most active catalysts for aqueous CO_2RR,[7–10] where abundant and nontoxic water can be used both as a solvent and as a proton source. Indeed, bicarbonate-based electrolytes are ubiquitous in these aqueous, heterogenous systems, where they have been shown to lead to higher CO_2RR efficiencies compared to other buffered electrolytes.[11–14]

Under aqueous conditions, CO_2 hydration establishes complex equilibria between dissolved CO_2, carbonic acid, bicarbonate, and carbonate.[11] In this context, the roles that bicarbonate (HCO_3^-) plays to enhance the CO_2RR at heterogeneous metal surfaces are debated. Although there is general consensus that bicarbonate is not a direct substrate for reduction, it has been proposed that it serves in a myriad of roles, including as a proton donor,[11–13,15] pH buffer,[7,12,16] or to facilitate an increase in the local concentration of CO_2 near the electrode surface through fast equilibrium between HCO_3^- and soluble CO_2 (Figure 1).[16] We hypothesized that bicarbonate may be similarly important in homogenous electrochemical systems operating in organic electrolytes; to the best of our knowledge, this topic has remained largely underexplored. We now report that templating bicarbonate binding in a well-defined molecular electrocatalysts using second-sphere coordination pendants can increase its acidity and enhance electrochemical CO_2 reduction.

RESULTS AND DISCUSSION

Design and Synthesis of Well-Defined Iron Porphyrin Catalysts Modified with Second-Sphere Urea Pendants to Template Bicarbonate Binding. To illustrate the general concept for this current study, we chose iron tetraphenylporphyrin (**Fe-TPP**) as a representative member of a prototypical class of molecular CO_2RR catalysts.[17–21] Inspired by the field of anion receptor chemistry,[22,23] we sought to enhance the interaction of the **Fe-TPP** catalyst with bicarbonate by incorporating a bis-aryl urea moiety into the second coordination sphere (Figure 1). (Thio)ureas are known to be highly effective motifs for selective binding of bicarbonate and other oxyanions, and thus have been incorporated into diverse frameworks such as amide-linked macrocycles,[24] cyclopeptide cages,[25] and tripodal[26] and linear[27–31] ligand scaffolds for recognition and sensing applications. Indeed, previous reports from our laboratory[6,32,33] and others[34–47] have established the ability of second coordination sphere pendants to enhance CO_2RR catalysis. As such, we reasoned that functionalization of **Fe-TPP** with a properly-positioned urea moiety would promote advantageous interactions with bicarbonate through templated hydrogen bonding interactions (Figure 1). Integration of urea moieties into porphyrin scaffolds to enhance CO_2 reduction through second-sphere hydrogen bonding interactions has been reported by Aukauloo and coworkers[48–51] but to the

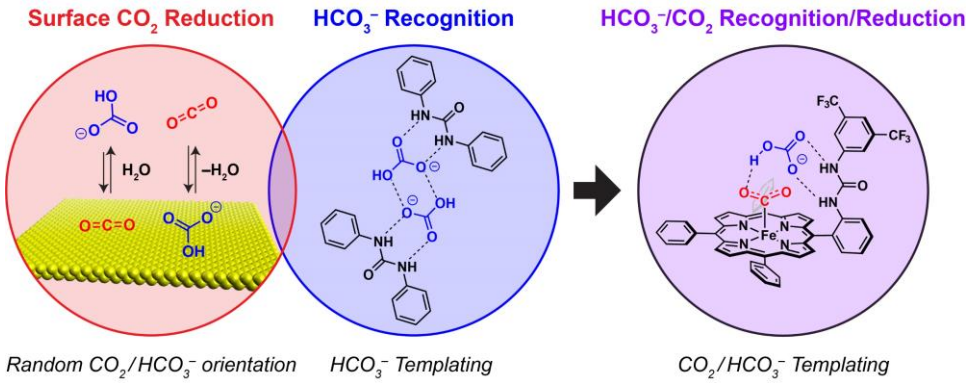

Figure 1. Templating bicarbonate in the second-coordination sphere of well-defined molecular catalysts can enhance the electrochemical carbon dioxide reduction reaction (CO_2RR). Merging the concept of the importance of bicarbonate-based aqueous electrolytes in heterogeneous CO_2RR with anion recognition in bis-aryl urea moieties can provide an effective design strategy for promoting homogeneous CO_2RR, as illustrated by the canonical iron porphyrin catalyst platform.

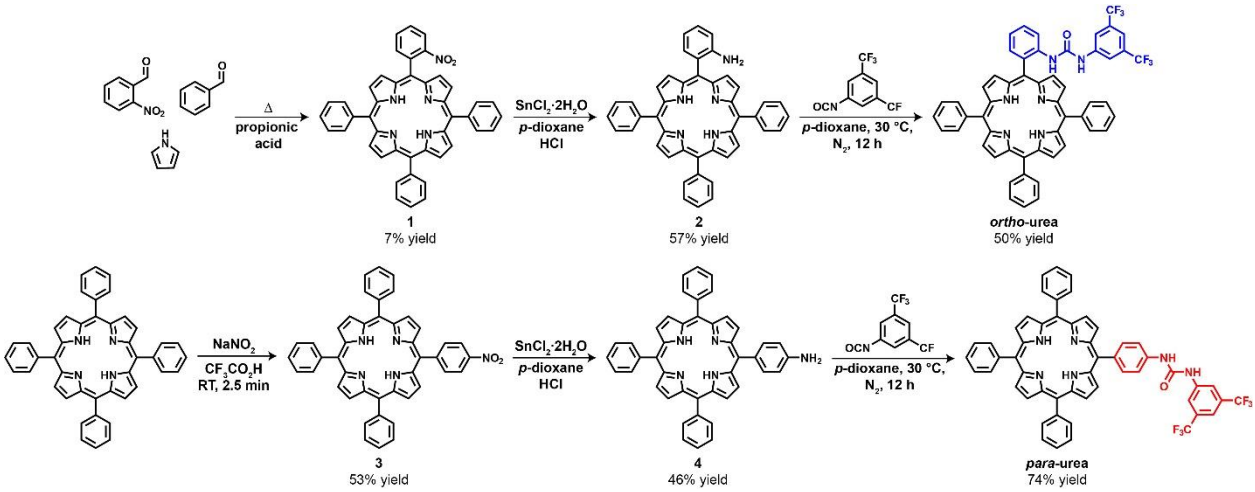

Scheme 1. Synthesis of *ortho*- and *para*-urea functionalized tetraphenylporphyrin ligands.

best of our knowledge, the anion recognition and templating properties of ureas has not been exploited in CO_2 reduction catalysis. We now show that proper positioning of this two-point hydrogen-bond moiety in the second sphere can promote bicarbonate-mediated CO_2RR in a well-defined molecular system.

Specifically, we targeted two positional isomers of urea-appended tetraphenylporphyrins, designated ***ortho*-urea** and ***para*-urea** according to the pendant's placement around the *meso* aryl ring. We predicted that the pendant group of **Fe-*ortho*-urea** would be located appropriately to enhance CO_2RR through direct interactions with Fe-bound CO_2 or by positioning a templated bicarbonate in the vicinity of the Fe active site, whereas the **Fe-*para*-urea** would serve as a positional negative control that was not expected to promote such effects. Synthesis of the functionalized porphyrins was achieved through a similar strategy utilized for amide analogs (Scheme 1).[32] Briefly, the *ortho* isomer was accessed through the condensation of 2-nitrobenzaldehyde, benzaldehyde, and pyrrole to give the mono-(2-nitrophenyl)porphyrin starting material (**1**). Reduction with tin chloride gave the subsequent amine, mono-(2-aminophenyl)porphyrin (**2**), and the reaction with 3,5-bis(trifluoromethyl)phenyl isocyanate afforded the target ***ortho*-urea** ligand. The *para* positional control was prepared from commercially available *meso*-tetraphenylporphyrin (TPP). Regioselective nitration of TPP with sodium nitrite in trifluoroacetic acid gave the corresponding mono-(4-nitrophenyl)porphyrin (**3**). Identical reduction and urea formation reaction conditions with tin chloride and 3,5-bis(trifluoromethyl)phenyl isocyanate, respectively, yielded the desired ***para*-urea** ligand. Metalation with iron bromide in anhydrous tetrahydrofuran with 2,6-lutidine as the base gave the desired urea-appended iron porphyrin complexes.

Structural Characterization Establishes the Ability of Urea Pendants to Poise Anions Proximal to the Porphyrin Metal Center. To establish connectivity and positioning of the urea moiety relative to the metal center, we sought to grow crystals suitable for X-ray diffraction analysis. Unfortunately, we were unable to obtain single crystals of **Fe-*ortho*-urea** due to severe twinning caused by stacking of the thin plate-shaped crystals. Instead, slow vapor diffusion of water into a concentrated DMF solution of the zinc analog, **Zn-*ortho*-urea,** produced diffraction-quality crystals (Figure 2, Table S1). As is typical for pentacoordinate Zn

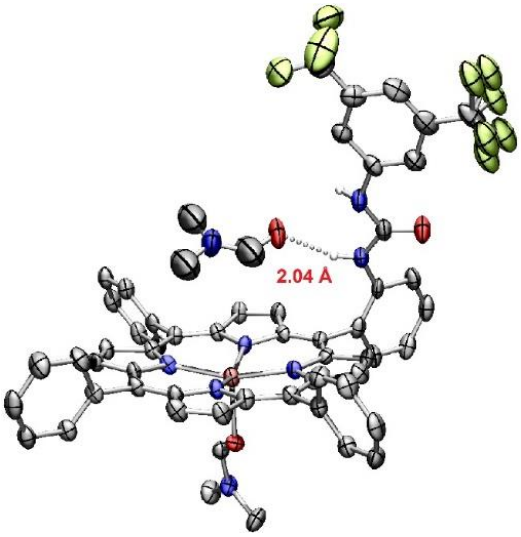

Figure 2. Solid-state structure of **Zn-*ortho*-urea** determined by single-crystal X-ray diffraction, showing the ability of a second-sphere urea pendant to poise an oxyanion proximal to the porphyrin metal center. Non-coordinated solvent molecules not participating in H-bonding interactions and C–H hydrogen atoms have been omitted for clarity. H-bonding is depicted by the dashed line. Brown, grey, blue, red, and green ellipsoids signify Zn, C, N, O, and F atoms, respectively. Thermal ellipsoids are plotted at the 50% probability level.

porphyrins, the Zn atom is axially coordinated to a DMF molecule causing displacement from the porphyrin plane by 0.331 Å. Unlike what was observed for the amide analog,[32] the urea moiety is engaged in tight hydrogen bonding with an exogenous DMF molecule and is distorted slightly from planarity in the solid state due to crystal packing interactions. The **Zn-*ortho*-urea** structure validates the ability of the urea pendant to form hydrogen bonding networks with solvent molecules and presumably also oxyanions such as bicarbonate.

Electrochemical Carbon Dioxide Reduction Catalyzed by Urea-Modified Iron Porphyrin Complexes. With the iron complexes in hand, we sought to evaluate their electrochemical properties under an inert atmosphere (Figure 3a). Cyclic voltammograms (CVs) for the urea-functionalized iron porphyrin complexes and **Fe-TPP** were measured in dry DMF electrolyte (0.10 M $TBAPF_6$, Figure 3a). Three distinct redox events are observed for all three complexes at approximately –0.6, –1.5, and –2.1 V *vs* Fc/Fc^+ corresponding to the formal Fe(III/II), Fe(II/I), and Fe(I/0) couples, respectively. At a scan rate of 100 mV/s, the Fe(I/0) couples exhibit chemically- and electrochemically reversible behavior. The Fe(I/0) standard potentials, E^0_{cat}, were determined under inert atmosphere by taking an average of three independent scans and are given in Table S2. CVs of **Fe-*ortho*-urea** and **Fe-*para*-urea** show additional redox waves apart from the three discussed above. Given the high affinity of urea moieties for halides,[52] we speculate that these additional waves may arise from electronically-distinct porphyrins where the urea is bound to Br^- or PF_6^-. Variable scan rate data collected for **Fe-*ortho*-urea** and **Fe-*para*-urea** establish that the peak cathodic currents are linearly correlated with the square root of the scan rate, indicating that these complexes are freely diffusing in solution (Figure S1).

Under a CO_2 atmosphere but with no added proton source, catalytic responses are observed for all three complexes, with **Fe-*ortho*-urea** exhibiting a much larger current enhancement relative to positional control **Fe-*para*-urea** and unmodified **Fe-TPP**. **Fe-*ortho*-urea** also displays significant curve-crossing behavior, where current on the return scan is higher than the current on the forward scan (Figure 3b, blue line). Curve-crossing is often indicative of an initial induction period where a more active catalytic species is generated *in situ* and thus its concentration increases as a function of time.[53] Interestingly, curve-crossing was not observed for **Fe-*para*-urea** or amide-functionalized analogs,[32] but has appeared in structurally-related urea porphyrins reported by Aukauloo and coworkers,[48–51] though they did not discuss this observation. Together, these data suggest that curve crossing depends on both the positioning and number of H-bond donors in the second coordination sphere, and hints that *ortho* urea groups engage in unique interactions during CO_2RR. Comparing the two control catalysts under CO_2, **Fe-*para*-urea** has a smaller catalytic response at more negative onset potential than **Fe-TPP**, which is unexpected given the electronic scaling relationship that exists between E^0_{cat} and catalytic rate, where catalysts with more negative E^0_{cat} values are expected to have greater driving force for CO_2 reduction.[54] A more detailed investigation of **Fe-*para*-urea** revealed that the observed rate constant for CO_2 reduction, k_{obs}, (obtained from Foot-of-the-Wave Analysis, FOWA, according to procedures described in the SI) exhibits first-order dependence on the catalyst concentration only at concentrations below 0.4 mM (Figure S2). At the higher concentrations used for cyclic voltammetric and preparative scale electrolysis experiments (*i.e.*, 1 mM), k_{obs} is inversely correlated with the concentration of **Fe-*para*-urea**, presumably due to a dimerization process occurring in solution (Figures S2). Similar dimers generated through H-bond templating with exogenous anions have been extensively observed for linear bis-urea ligands,[27] which may explain the lower-than-expected observed activity of **Fe-*para*-urea**.

Positional Effects of Second-Sphere Urea Pendants on Bicarbonate-Mediated Enhancement of Electrochemical Carbon Dioxide Reduction. Given our hypotheses regarding the important roles of bicarbonate in non-aqueous CO_2RR and the possible templating ability of the pendant urea, we examined how the catalytic responses of our porphyrins change upon addition of tetraethylammonium bicarbonate ($TEAHCO_3$) in DMF electrolyte ($TBAPF_6$). Titration of $TEAHCO_3$ into a solution of **Fe-*ortho*-urea** under CO_2 atmosphere results in a large enhancement in the catalytic wave (Figure 3c). Interestingly, the curve-crossing behavior was eliminated at higher concentrations of bicarbonate (~10 mM). Comparison of the catalytic performance of **Fe-*ortho*-urea** to **Fe-*para*-urea** and **Fe-TPP** in the presence of $TEAHCO_3$ is provided in Figure 3. The data show that titration of $TEAHCO_3$ into a CO_2-saturated solution of **Fe-*para*-urea** or **Fe-TPP** (Figure S4) also results in a catalytic enhancement, but much less than what is observed for **Fe-*ortho*-urea** (Figure S5). Interestingly, the titration of

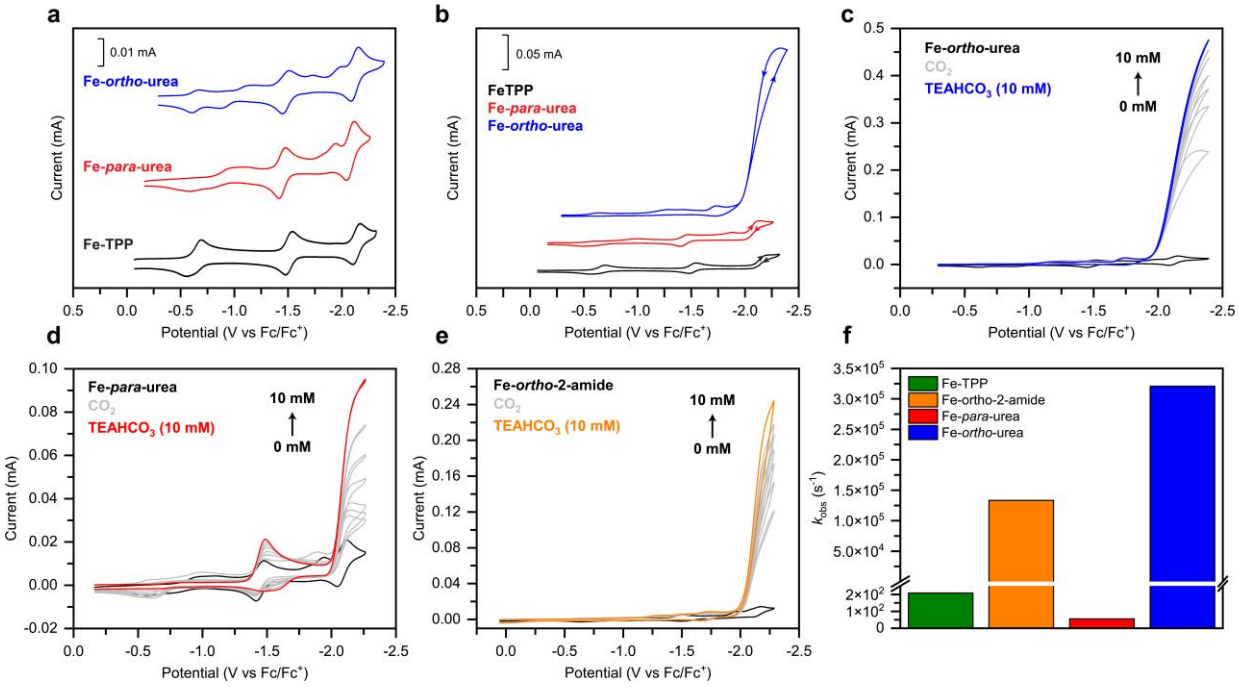

Figure 3. Electrochemical analysis of iron porphyrin complexes. Cyclic voltammograms (CVs) of **Fe-TPP** (black), **Fe-*para*-urea** (red), and **Fe-*ortho*-urea** (blue) under (a) Ar and (b) CO_2 atmosphere, showing a marked catalytic current enhancement for the *ortho* analog. Comparison of the catalytic performance of iron porphyrin complexes under CO_2 atmosphere in the presence of bicarbonate. Titrations of $TEAHCO_3$ into solutions of (c) **Fe-*ortho*-urea**, (d) **Fe-*para*-urea**, and (e) **Fe-*ortho*-2-amide** show a marked enhancement of catalytic activity with this additive. (f) Direct comparison of the observed rate constants (k_{obs}) extracted from FOWA of the iron porphyrin complexes under CO_2 saturated electrolyte with 10 mM $TEAHCO_3$ show that the **Fe-*ortho*-urea** has the largest current enhancement, with a 1500-fold increase over **Fe-TPP**. Conditions: 0.1 M $TBAPF_6$ in DMF, 1 mM Fe complexes, 0 – 10 mM $TEAHCO_3$, 100 mV/s scan rate.

$TEAHCO_3$ into a solution of our previously reported **Fe-*ortho*-2-amide** catalyst[32] under a CO_2 atmosphere also results in a large increase in the catalytic current (Figure 3e). Thus, it appears that bicarbonate addition results in a generalizable enhancement in catalytic activity with iron porphyrin catalysts, suggesting that bicarbonate may function as a proton donor under these conditions.

Surprisingly, we were unable to find a reported pK_a value for HCO_3^- in non-aqueous media and therefore measured this value experimentally using a spectrophotometric method; we determined the pK_a of $TEAHCO_3$ in DMSO to be 20.8 ± 0.1 (Figure S12). This result supports the notion that bicarbonate acts as the principal proton source under our electrolysis conditions. Furthermore, we note that the pK_a (DMSO) of HCO_3^- is comparable to other typical acids for electrochemical CO_2RR in organic solution such as phenol (18.0), 2,2,2-trifluoroethanol (23.6), and water (32.0).[55] As such, we sought to consider the role of equilibria involving HCO_3^-, including the concentration of basic additives or residual water in a non-aqueous electrolyte.

To determine the selectivity and stability for electrochemical CO_2 reduction, preparative-scale controlled potential electrolysis (CPE) experiments were conducted in a CO_2-saturated gas-tight H-cell with and without the addition of 100 mM $TEAHCO_3$ (Figures S6 and S7, Table S3). The urea-appended catalysts are stable during catalysis, with steady current density maintained across the hour-long CPE experiments. At the same applied potential of -2.18 V *vs* Fc/Fc^+, **Fe-*ortho*-urea** operates at much higher current densities (1.61 mA/cm^2) compared to **Fe-*para*-urea** (0.37 mA/cm^2). Moreover, we also observe a stark difference in Faradaic efficiency for CO production (FE_{CO}): **Fe-*ortho*-urea** achieves an average FE_{CO} of 98% while **Fe-*para*-urea** achieves an average FE_{CO} of only 3%. Addition of $TEAHCO_3$ (100 mM) causes the average current density of **Fe-*ortho*-urea** and **Fe-*para*-urea** to increase to 3.08 mA/cm^2 and 0.98 mA/cm^2, respectively, and are indicative of a large catalytic rate enhancement due to the bicarbonate additive. **Fe-*ortho*-urea** maintains a high FE_{CO} in the presence of $TEAHCO_3$ (93%) while the FE_{CO} for **Fe-*para*-urea** increases to 54%. No H_2 (or a trace amount) is detected for either catalyst under either of these conditions (Table S3). We speculate that the low FE_{CO} observed for the *para*-functionalized analog may be due to its propensity to dimerize into a catalytically-inactive form *(vide supra)*, where hydrogen bonding between the urea moiety and bicarbonate may disrupt formation of this dimer and lead to an improvement in FE_{CO}.

Having confirmed that CO is the unique catalytic product of electrochemical CO_2RR, we turned to Foot-of-the-Wave Analysis (FOWA) to obtain quantitative catalytic metrics. Observed catalytic rate constants (k_{obs}) of the iron porphyrin complexes were determined using FOWA in the presence of 0-10 mM $TEAHCO_3$ (limiting) and 0.23 M CO_2 (excess) (Figures S8–S11). The data show that catalysis has approximately first-order dependence on bicarbonate concentration for most of the iron porphyrins investigated. Figure 3f shows a comparison of k_{obs} values at [$TEAHCO_3$] = 10

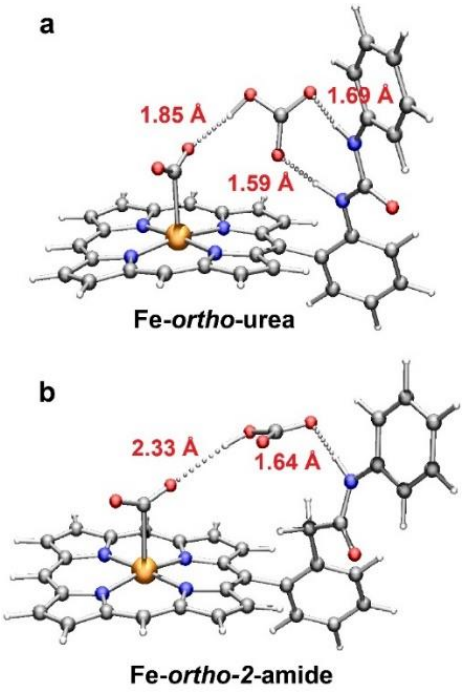

Figure 4. Optimized structures from DFT (B97-D)[56] calculations of Fe(0)–CO_2 adducts of (a) **Fe-*ortho*-urea** and (b) **Fe-*ortho*-2-amide**,[32] with bicarbonate to probe the H-bond templating of bicarbonate to iron porphyrin scaffolds employing either a 1-point or 2-point H-bond donor. The geometry optimized structure for the *para*-urea control is given in Figure S14. Orange, grey, blue, white, and red atoms signify Fe, C, N, H, and O, respectively. To reduce computational cost, the ligands were truncated to remove the non-functionalized phenyl moieties and the bis(3,5-trifluoromethyl) functional groups. The DFT calculations support the importance of the two-point urea binder to properly position bicarbonate relative to the Fe(0)–CO_2 adduct for substrate reduction as well as increase the acidity of bicarbonate as an acid to facilitate proton transfer in CO_2RR.

mM and illustrates that proper positioning of the urea moiety increases k_{obs} by three to four orders of magnitude over parent **Fe-TPP**. The number of hydrogen bond donors also influences catalytic rates, with the two-point H-bond donor **Fe-*ortho*-urea** exhibiting a greater than two-fold improvement in k_{obs} relative to its one-point counterpart **Fe-*ortho*-2-amide**.

Second-Sphere Urea Pendants Increase Acidity of Templated Bicarbonate as a Proton Source to Promote Carbon Dioxide Reduction. We hypothesized that the *ortho* urea group engages in hydrogen bonding with bicarbonate and that this interaction enhances CO_2RR catalysis by 1) templating the bicarbonate proton close to CO_2-bound intermediates and 2) further lowering the pK_a of bicarbonate, thereby increasing the driving force for proton transfer. We first evaluated the binding of bicarbonate to the free-base *ortho*-urea ligand by ^{1}H NMR (Figure S13). Sub-stoichiometric titration of $TEAHCO_3$ causes an upfield shift of the aryl resonances and a complete loss of the urea-proton signals due to fast exchange with the bicarbonate proton. The control titration of $TEAHCO_3$ into a solution of unmodified TPP displays no spectral change, even upon the addition of excess bicarbonate, illustrating the strong interaction between the urea moiety and bicarbonate in solution. The interaction between bicarbonate and the porphyrins was further investigated by density functional theory (DFT) (Figure 4). DFT calculations show that bicarbonate does indeed hydrogen bond tightly to the urea moiety in a bidentate fashion that is not possible for the amide analog (Figure 4).[32] When the urea is in the *ortho*-position, the hydrogen bonding network positions the bicarbonate proton close (1.85 Å) to the iron-bound CO_2 moiety. This urea-templated bicarbonate binding effectively dangles its proton close to CO_2, enabling stabilization of the transition state and/or promoting proton transfer. This templating effect is not possible with only one hydrogen bond donor as the bicarbonate proton is positioned much further away from the CO_2-bound intermediate in the amide case (~2.33 Å). DFT calculations further predict the pK_a of bicarbonate to decrease by ~5.5 (relative to free HCO_3^-) due to this templated hydrogen bonding with **Fe-*ortho*-urea**. These computational results support a model in which the **Fe-*ortho*-urea** complex displays the largest catalytic enhancement owing to its ability to template and activate bicarbonate by synergistic second-sphere interactions. Taken together, these results suggest that the curve-crossing behavior may arise from changes to $CO_2/HCO_3^-/CO_3^{-2}$ equilibria in the diffusion layer over the time course of a CV scan. The kinetics of CO_2 hydration to generate HCO_3^- are relatively slow, so initial CO_2 reduction with **Fe-*ortho*-urea** likely proceeds *via* a slower proton-limited pathway where one CO_2 molecule serves as a Lewis acid to activate the reduced CO_2, generating CO and CO_3^{2-} as products.[20] Diffusion-controlled proton transfer from adventitious water then rapidly generates HCO_3^-, which is templated and activated by the pendant urea group and helps promote a faster catalytic pathway with bicarbonate as the proton donor.

CONCLUDING REMARKS

In summary, we have shown that bicarbonate, as an additive, causes a large catalytic enhancement in homogenous electrochemical CO_2 reduction in organic electrolyte. Using iron porphyrin as a representative molecular catalyst platform, installation of a properly positioned urea moiety into the second coordination sphere as a bicarbonate anion receptor further facilitates a marked improvement in catalytic rates. Spectrophotometric pK_a measurements, NMR binding studies, and DFT calculations provide support that bicarbonate operates as a competent proton donor and that templated binding to the urea results in the generation of a much stronger acid that is appropriately positioned for rapid proton transfer to a CO_2-bound intermediate. Taken together, this study identifies the importance of understanding the CO_2/HCO_3^- solution equilibria under organic electrolyte conditions where molecular catalysts are often utilized and shows how the second coordination sphere can be designed to exploit these equilibria for CO_2RR catalysis.

ASSOCIATED CONTENT

Supporting Information. Experimental and computational details, supplemental electrochemical and DFT geometry optimized atomic xyz coordinates is available free of charge via the Internet at http://pubs.acs.org.

AUTHOR INFORMATION

Corresponding Authors

***Christopher J. Chang** – Departments of Chemistry and Molecular and Cell Biology University of California, Berkeley, CA, 94720, USA; Chemical Sciences Division, Lawrence Berkeley National Laboratory, Berkeley, CA, 94720, USA. orcid.org/0000-0001-5732-9497; chrischang@berkeley.edu

***Eva M. Nichols** – Department of Chemistry, The University of British Columbia, Vancouver, BC, V6T 1Z1, Canada; orcid.org/0000-0002-3718-7273; enichols@chem.ubc.ca

Authors

Jeffrey S. Derrick – Department of Chemistry University of California, Berkeley, CA, 94720, USA; Chemical Sciences Division, Lawrence Berkeley National Laboratory, Berkeley, CA, 94720, USA. orcid.org/0000-0002-3879-2897.

Matthias Loipersberger – Department of Chemistry University of California, Berkeley, CA, 94720, USA. orcid.org/0000-0002-3648-0101.

Sepand K. Nistanaki – Department of Chemistry University of California, Berkeley, CA, 94720, USA. orcid.ord/0000-0002-803X

Martin Head-Gordon – Department of Chemistry University of California, Berkeley, CA, 94720, USA; Chemical Sciences Division, Lawrence Berkeley National Laboratory, Berkeley, CA, 94720, USA. orcid.org/0000-0002-4309-6669.

ACKNOWLEDGMENT

This work was supported by the U.S. Department of Energy, Office of Science, Office of Advanced Scientific Computing, Office of Basic Energy Sciences, via the Division of Chemical Sciences, Geosciences, and Bioscience of the U.S. Department of Energy at Lawrence Berkeley National Laboratory (Grant No. DE-AC02-05CH11231 to C.J.C.) and via the Scientific Discovery through Advanced Computing (SciDAC) program (M.H.G.). J.S.D. thanks Chevron for a graduate fellowship. E.M.N. acknowledges the NSF for a Graduate Research Fellowship. C.J.C. is a CIFAR Fellow.

REFERENCES

(1) Appel, A. M.; Bercaw, J. E.; Bocarsly, A. B.; Dobbek, H.; DuBois, D. L.; Dupuis, M.; Ferry, J. G.; Fujita, E.; Hille, R.; Kenis, P. J. A.; Kerfeld, C. A.; Morris, R. H.; Peden, C. H. F.; Portis, A. R.; Ragsdale, S. W.; Rauchfuss, T. B.; Reek, J. N. H.; Seefeldt, L. C.; Thauer, R. K.; Waldrop, G. L. Frontiers, Opportunities, and Challenges in Biochemical and Chemical Catalysis of CO_2 Fixation. *Chem. Rev.* **2013**, *113*, 6621–6658.

(2) Benson, E. E.; Kubiak, C. P.; Sathrum, A. J.; Smieja, J. M. Electrocatalytic and Homogeneous Approaches to Conversion of CO_2 to Liquid Fuels. *Chem. Soc. Rev.* **2008**, *38*, 89–99.

(3) Lewis, N. S.; Nocera, D. G. Powering the Planet: Chemical Challenges in Solar Energy Utilization. *Proc. Natl. Acad. Sci.* **2006**, *103*, 15729–15735.

(4) De Luna, P.; Hahn, C.; Higgins, D.; Jaffer, S. A.; Jaramillo, T. F.; Sargent, E. H. What Would It Take for Renewably Powered Electrosynthesis to Displace Petrochemical Processes? *Science* **2019**, *364*, eaav3506.

(5) Francke, R.; Schille, B.; Roemelt, M. Homogeneously Catalyzed Electroreduction of Carbon Dioxide—Methods, Mechanisms, and Catalysts. *Chem. Rev.* **2018**, *118*, 4631–4701.

(6) Smith, P. T.; Nichols, E. M.; Cao, Z.; Chang, C. J. Hybrid Catalysts for Artificial Photosynthesis: Merging Approaches from Molecular, Materials, and Biological Catalysis. *Acc. Chem. Res.* **2020**, *53*, 575–587.

(7) Hori, Y. Electrochemical CO_2 Reduction on Metal Electrodes. In *Modern Aspects of Electrochemistry*; Vayenas, C. G., White, R. E., Gamboa-Aldeco, M. E., Eds.; Modern Aspects of Electrochemistry; Springer: New York, NY, 2008; pp 89–189.

(8) Zhao, S.; Jin, R.; Jin, R. Opportunities and Challenges in CO_2 Reduction by Gold- and Silver-Based Electrocatalysts: From Bulk Metals to Nanoparticles and Atomically Precise Nanoclusters. *ACS Energy Lett.* **2018**, *3*, 452–462.

(9) Nitopi, S.; Bertheussen, E.; Scott, S. B.; Liu, X.; Engstfeld, A. K.; Horch, S.; Seger, B.; Stephens, I. E. L.; Chan, K.; Hahn, C.; Nørskov, J. K.; Jaramillo, T. F.; Chorkendorff, I. Progress and Perspectives of Electrochemical CO_2 Reduction on Copper in Aqueous Electrolyte. *Chem. Rev.* **2019**, *119*, 7610–7672.

(10) Proppe, A. H.; Li, Y. C.; Aspuru-Guzik, A.; Berlinguette, C. P.; Chang, C. J.; Cogdell, R.; Doyle, A. G.; Flick, J.; Gabor, N. M.; van Grondelle, R.; Hammes-Schiffer, S.; Jaffer, S. A.; Kelley, S. O.; Leclerc, M.; Leo, K.; Mallouk, T. E.; Narang, P.; Schlau-Cohen, G. S.; Scholes, G. D.; Vojvodic, A.; Yam, V. W.-W.; Yang, J. Y.; Sargent, E. H. Bioinspiration in Light Harvesting and Catalysis. *Nat. Rev. Mater.* **2020**, *5*, 828–846.

(11) Wuttig, A.; Yoon, Y.; Ryu, J.; Surendranath, Y. Bicarbonate Is Not a General Acid in Au-Catalyzed CO_2 Electroreduction. *J. Am. Chem. Soc.* **2017**, *139*, 17109–17113.

(12) Marcandalli, G.; Villalba, M.; Koper, M. T. M. The Importance of Acid–Base Equilibria in Bicarbonate Electrolytes for CO_2 Electrochemical Reduction and CO Reoxidation Studied on Au(hkl) Electrodes. *Langmuir* **2021**, *37*, 5707–5716.

(13) Zeng, J. S.; Corbin, N.; Williams, K.; Manthiram, K. Kinetic Analysis on the Role of Bicarbonate in Carbon Dioxide Electroreduction at Immobilized Cobalt Phthalocyanine. *ACS Catal.* **2020**, *10*, 4326–4336.

(14) Li, T.; Lees, E. W.; Goldman, M.; Salvatore, D. A.; Weekes, D. M.; Berlinguette, C. P. Electrolytic Conversion of Bicarbonate into CO in a Flow Cell. *Joule* **2019**, *3*, 1487–1497.

(15) Chen, Y.; Li, C. W.; Kanan, M. W. Aqueous CO_2 Reduction at Very Low Overpotential on Oxide-Derived Au Nanoparticles. *J. Am. Chem. Soc.* **2012**, *134*, 19969–19972.

(16) Dunwell, M.; Lu, Q.; Heyes, J. M.; Rosen, J.; Chen, J. G.; Yan, Y.; Jiao, F.; Xu, B. The Central Role of Bicarbonate in the Electrochemical Reduction of Carbon Dioxide on Gold. *J. Am. Chem. Soc.* **2017**, *139*, 3774–3783.

(17) Takahashi, K.; Hiratsuka, K.; Sasaki, H.; Toshima, S. Electrocatalytic Behavior of Metal Porphyrins in the Reduction of Carbon Dioxide. *Chem. Lett.* **1979**, *8*, 305–308.

(18) Hammouche, M.; Lexa, D.; Savéant, J. M.; Momenteau, M. Catalysis of the Electrochemical Reduction of Carbon Dioxide by Iron("0") Porphyrins. *J. Electroanal. Chem. Interfacial Electrochem.* **1988**, *249*, 347–351.

(19) Hammouche, M.; Lexa, D.; Momenteau, M.; Saveant, J. M. Chemical Catalysis of Electrochemical Reactions. Homogeneous Catalysis of the Electrochemical Reduction of Carbon Dioxide by Iron("0") Porphyrins. Role of the Addition of Magnesium Cations. *J. Am. Chem. Soc.* **1991**, *113*, 8455–8466.

(20) Bhugun, I.; Lexa, D.; Savéant, J.-M. Catalysis of the Electrochemical Reduction of Carbon Dioxide by Iron(0) Porphyrins: Synergystic Effect of Weak Brönsted Acids. *J. Am. Chem. Soc.* **1996**, *118*, 1769–1776.

(21) Behar, D.; Dhanasekaran, T.; Neta, P.; Hosten, C. M.; Ejeh, D.; Hambright, P.; Fujita, E. Cobalt Porphyrin Catalyzed Reduction of CO_2. Radiation Chemical, Photochemical, and Electrochemical Studies. *J. Phys. Chem. A* **1998**, *102*, 2870–2877.

(22) Evans, N. H.; Beer, P. D. Advances in Anion Supramolecular Chemistry: From Recognition to Chemical Applications. *Angew. Chem. Int. Ed.* **2014**, *53*, 11716–11754.

(23) Chen, L.; Berry, S. N.; Wu, X.; Howe, E. N. W.; Gale, P. A. Advances in Anion Receptor Chemistry. *Chem* **2020**, *6*, 61–141.

(24) Brooks, S. J.; Gale, P. A.; Light, M. E. Anion-Binding Modes in a Macrocyclic Amidourea. *Chem. Commun.* **2006**, 4344–4346.

(25) Busschaert, N.; Karagiannidis, L. E.; Wenzel, M.; Haynes, C. J. E.; Wells, N. J.; Young, P. G.; Makuc, D.; Plavec, J.; Jolliffe, K. A.; Gale, P. A. Synthetic Transporters for Sulfate: A New Method for the Direct Detection of Lipid Bilayer Sulfate Transport. *Chem. Sci.* **2014**, *5*, 1118–1127.

(26) Busschaert, N.; Gale, P. A.; Haynes, C. J. E.; Light, M. E.; Moore, S. J.; Tong, C. C.; Davis, J. T.; William A. Harrell, J. Tripodal Transmembrane Transporters for Bicarbonate. *Chem. Commun.* **2010**, *46*, 6252–6254.

(27) Manna, U.; Das, A.; Das, G. Self-Assemblies of Positional Isomeric Linear Bis-Urea Ligands with Oxyanions/Hydrated Oxyanions: Evidence of F^- and OH^- Induced Atmospheric CO_2 Fixation. *Cryst. Growth Des.* **2018**, *18*, 6801–6815.

(28) Brooks, S. J.; Edwards, P. R.; Gale, P. A.; Light, M. E. Carboxylate Complexation by a Family of Easy-to-Make Ortho-Phenylenediamine Based Bis-Ureas: Studies in Solution and the Solid State. *New J. Chem.* **2006**, *30*, 65–70.

(29) Moore, S. J.; Haynes, C. J. E.; González, J.; Sutton, J. L.; Brooks, S. J.; Light, M. E.; Herniman, J.; Langley, G. J.; Soto-Cerrato, V.; Pérez-Tomás, R.; Marques, I.; Costa, P. J.; Félix, V.; Gale, P. A. Chloride, Carboxylate, and Carbonate Transport by Ortho-Phenylenediamine-Based Bisureas. *Chem Sci* **2013**, *4*, 103–117.

(30) Manna, U.; Kayal, S.; Nayak, B.; Das, G. Systematic Size Mediated Trapping of Anions of Varied Dimensionality within a Dimeric Capsular Assembly of a Flexible Neutral Bis-Urea Platform. *Dalton Trans.* **2017**, *46*, 11956–11969.

(31) Manna, U.; Kayal, S.; Samanta, S.; Das, G. Fixation of Atmospheric CO_2 as Novel Carbonate–$(Water)_2$–Carbonate Cluster and Entrapment of Double Sulfate within a Linear Tetrameric Barrel of a Neutral Bis-Urea Scaffold. *Dalton Trans.* **2017**, *46*, 10374–10386.

(32) Nichols, E. M.; Derrick, J. S.; Nistanaki, S. K.; Smith, P. T.; Chang, C. J. Positional Effects of Second-Sphere Amide Pendants on Electrochemical CO_2 Reduction Catalyzed by Iron Porphyrins. *Chem. Sci.* **2018**, *9*, 2952–2960.

(33) Nichols, E. M.; Chang, C. J. Urea-Based Multipoint Hydrogen-Bond Donor Additive Promotes Electrochemical CO_2 Reduction Catalyzed by Nickel Cyclam. *Organometallics* **2019**, *38*, 1213–1218.

(34) Costentin, C.; Drouet, S.; Robert, M.; Savéant, J.-M. A Local Proton Source Enhances CO_2 Electroreduction to CO by a Molecular Fe Catalyst. *Science* **2012**, *338*, 90–94.

(35) Costentin, C.; Passard, G.; Robert, M.; Savéant, J.-M. Ultraefficient Homogeneous Catalyst for the CO_2-to-CO Electrochemical Conversion. *Proc. Natl. Acad. Sci.* **2014**, *111*, 14990–14994.

(36) Azcarate, I.; Costentin, C.; Robert, M.; Savéant, J.-M. Through-Space Charge Interaction Substituent Effects in Molecular Catalysis Leading to the Design of the Most Efficient Catalyst of CO_2-to-CO Electrochemical Conversion. *J. Am. Chem. Soc.* **2016**, *138*, 16639–16644.

(37) Kinzel, N. W.; Werlé, C.; Leitner, W. Transition Metal Complexes as Catalysts for the Electroconversion of CO_2: An Organometallic Perspective. *Angew. Chem. Int. Ed.* **2021**, *60*, 11628–11686.

(38) Drover, M. W. A Guide to Secondary Coordination Sphere Editing. *Chem. Soc. Rev.* **2022**.

(39) Haviv, E.; Azaiza-Dabbah, D.; Carmieli, R.; Avram, L.; Martin, J. M. L.; Neumann, R. A Thiourea Tether in the Second Coordination Sphere as a Binding Site for CO_2 and a Proton Donor Promotes the Electrochemical Reduction of CO_2 to CO Catalyzed by a Rhenium Bipyridine-Type Complex. *J. Am. Chem. Soc.* **2018**, *140*, 12451–12456.

(40) Sen, P.; Mondal, B.; Saha, D.; Rana, A.; Dey, A. Role of 2nd Sphere H-Bonding Residues in Tuning the Kinetics of CO_2 Reduction to CO by Iron Porphyrin Complexes. *Dalton Trans.* **2019**, *48*, 5965–5977.

(41) Amanullah, S.; Saha, P.; Dey, A. Activating the Fe(I) State of Iron Porphyrinoid with Second-Sphere Proton Transfer Residues for Selective Reduction of CO_2 to HCOOH via Fe(III/II)–COOH Intermediate(s). *J. Am. Chem. Soc.* **2021**, *143*, 13579–13592.

(42) Johnson, E. M.; Liu, J. J.; Samuel, A. D.; Haiges, R.; Marinescu, S. C. Switching Catalyst Selectivity via the Introduction of a Pendant Nitrophenyl Group. *Inorg. Chem.* **2022**, *61*, 1316–1326.

(43) Chapovetsky, A.; Liu, J. J.; Welborn, M.; Luna, J. M.; Do, T.; Haiges, R.; Miller III, T. F.; Marinescu, S. C. Electronically Modified Cobalt Aminopyridine Complexes Reveal an Orthogonal Axis for Catalytic Optimization for CO_2 Reduction. *Inorg. Chem.* **2020**, *59*, 13709–13718.

(44) Chapovetsky, A.; Welborn, M.; Luna, J. M.; Haiges, R.; Miller, T. F.; Marinescu, S. C. Pendant Hydrogen-Bond Donors in Cobalt Catalysts Independently Enhance CO_2 Reduction. *ACS Cent. Sci.* **2018**, *4*, 397–404.

(45) Yang, J. Y.; Smith, S. E.; Liu, T.; Dougherty, W. G.; Hoffert, W. A.; Kassel, W. S.; DuBois, M. R.; DuBois, D. L.; Bullock, R. M. Two Pathways for Electrocatalytic Oxidation of Hydrogen by a Nickel Bis(Diphosphine) Complex with Pendant Amines in the Second Coordination Sphere. *J. Am. Chem. Soc.* **2013**, *135*, 9700–9712.

(46) Margarit, C. G.; Asimow, N. G.; Gonzalez, M. I.; Nocera, D. G. Double Hangman Iron Porphyrin and the Effect of Electrostatic Nonbonding Interactions on Carbon Dioxide Reduction. *J. Phys. Chem. Lett.* **2020**, *11*, 1890–1895.

(47) Margarit, C. G.; Schnedermann, C.; Asimow, N. G.; Nocera, D. G. Carbon Dioxide Reduction by Iron Hangman Porphyrins. *Organometallics* **2019**, *38*, 1219–1223.

(48) Gotico, P.; Boitrel, B.; Guillot, R.; Sircoglou, M.; Quaranta, A.; Halime, Z.; Leibl, W.; Aukauloo, A. Second-Sphere Biomimetic Multipoint Hydrogen-Bonding Patterns to Boost CO_2 Reduction of Iron Porphyrins. *Angew. Chem. Int. Ed.* **2019**, *58*, 4504–4509.

(49) Gotico, P.; Roupnel, L.; Guillot, R.; Sircoglou, M.; Leibl, W.; Halime, Z.; Aukauloo, A. Atropisomeric Hydrogen Bonding Control for CO_2 Binding and Enhancement of Electrocatalytic Reduction at Iron Porphyrins. *Angew. Chem. Int. Ed.* **2020**, *59*, 22451–22455.

(50) Khadhraoui, A.; Gotico, P.; Leibl, W.; Halime, Z.; Aukauloo, A. Through-Space Electrostatic Interactions Surpass Classical Through-Bond Electronic Effects in Enhancing CO_2 Reduction Performance of Iron Porphyrins. *ChemSusChem* **2021**, *14*, 1308–1315.

(51) Zhang, C.; Dragoe, D.; Brisset, F.; Boitrel, B.; Lassalle-Kaiser, B.; Leibl, W.; Halime, Z.; Aukauloo, A. Second-Sphere Hydrogen-Bonding Enhances Heterogeneous Electrocatalytic CO_2 to CO Reduction by Iron Porphyrins in Water. *Green Chem.* **2021**, *23*, 8979–8987.

(52) Zhang, Z.; Schreiner, P. R. (Thio)Urea Organocatalysis—What Can Be Learnt from Anion Recognition? *Chem. Soc. Rev.* **2009**, *38*, 1187.

(53) Lee, K. J.; McCarthy, B. D.; Dempsey, J. L. On Decomposition, Degradation, and Voltammetric Deviation: The Electrochemist's Field Guide to Identifying Precatalyst Transformation. *Chem. Soc. Rev.* **2019**, *48*, 2927–2945.

(54) Costentin, C.; Savéant, J.-M. Homogeneous Molecular Catalysis of Electrochemical Reactions: Manipulating Intrinsic and Operational Factors for Catalyst Improvement. *J. Am. Chem. Soc.* **2018**, *140*, 16669–16675.

(55) Bordwell, F. G. Equilibrium Acidities in Dimethyl Sulfoxide Solution. *Acc. Chem. Res.* **1988**, *21* (12), 456–463.

(56) Antony, J.; Grimme, S. Density Functional Theory Including Dispersion Corrections for Intermolecular Interactions in a Large Benchmark Set of Biologically Relevant Molecules. *Phys. Chem. Chem. Phys.* **2006**, *8* (45), 5287–5293.

TOC:

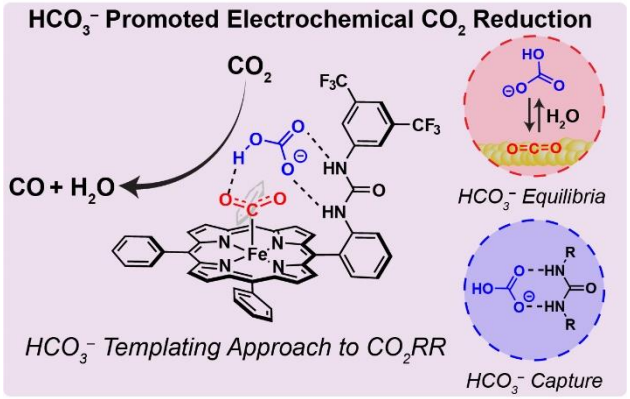
HCO3- Promoted Electrochemical CO2 Reduction
CO2
CO + H2O
F3C
CF3
HN
HN
O
H
O
O
O=C=O
Fe
N
N
N
N
HO
H2O
O=C=O
HCO3- Equilibria
R
HO
HN
HN
R
HCO3- Templating Approach to CO2RR
HCO3- Capture